

Insights on the High-Temperature Operational Limits of $\text{ZrO}_2\text{-Y}_2\text{O}_3$ TBCs Manufactured via Air Plasma Spray

Rogério S. Lima and Basil R. Marple

(Submitted October 12, 2016; in revised form January 5, 2017; published online February 15, 2017)

The effective high-temperature operation limit of a $\text{ZrO}_2\text{-7-8 wt.\%Y}_2\text{O}_3$ (YSZ) thermal barrier coating (TBC) manufactured via air plasma spray (APS) is considered to be $\sim 1300^\circ\text{C}$. This is related to the metastable tetragonal \prime -phase formed during the rapid quenching of the YSZ particles during spraying. The \prime -phase transforms into the equilibrium tetragonal and cubic phases at temperatures $\geq \sim 1300^\circ\text{C}$, which can lead to the formation of the monoclinic phase of YSZ upon cooling to room temperature. This formation of the monoclinic phase is accompanied by a volume expansion that leads to TBC failure due to extensive micro-cracking. To further investigate this limitation, an APS YSZ TBC was sprayed on a CMSX-4 substrate. By using a thermal (laser) gradient cyclic testing, a temperature gradient was generated across the TBC/substrate system. The YSZ *T-front* and substrate backside *T-back* temperature levels were ~ 1500 and $\sim 1000^\circ\text{C}$, respectively. In cycle conditions (5-min or 1-h hot and 2-min cool), no TBC failure has been observed. This behavior was partially attributed to the unexpected absence of the monoclinic phase of the YSZ in the cycled coatings. Although preliminary, these results are promising regarding increasing the effective high-temperature operational limits of APS YSZ TBCs.

Keywords aerospace, air plasma spray (APS), life prediction, thermal barrier coating (TBC), thermal conductivity, thermal gradient cyclic testing, $\text{ZrO}_2\text{-7-8 wt.\%Y}_2\text{O}_3$ (YSZ)

1. Introduction

Thermal barrier coatings (TBCs) deposited via thermal spray processing are applied onto the static metallic superalloy parts of the hot zones of jet turbine engines (e.g., combustion chambers, vanes and afterburners) to protect them against excessive heat of the combustion gases (Ref 1). In addition, TBCs can also be used in other types of aerospace applications, such as, on the internal diameters (IDs) of the exhaust nozzles of rocket engines (Ref 2).

An as-sprayed TBC system typically exhibits a bilayered structure, i.e., a ceramic top coat (e.g., $\text{ZrO}_2\text{-8 wt.\%Y}_2\text{O}_3$, a.k.a., YSZ) and a metallic MCrAlY bond coat (BC) (M=Ni, Co, NiCo or CoNi) deposited onto a metallic superalloy substrate (Ref 3, 4). As pointed out by Feuerstein et al. (Ref 4), the thicknesses of aerospace turbine TBCs are typically 125–250 μm and 250–500 μm for the BC and YSZ top coat, respectively. The thicknesses of the metallic superalloy walls of combustion chambers are generally found within the range of $\sim 1\text{-}2$ mm.

Air plasma spray (APS) processing is the standard technique employed to deposit the YSZ top coat. The MCrAlY BCs can be deposited by different thermal spray systems. However, the APS technique is the workhorse system to spray BCs, mainly for IDs of combustion chambers and afterburners. This is

related to the typical small sizes of APS torches when compared to the other types of thermal spray torches, i.e., APS torches typically can be easily fitted for ID spraying.

The main role of the MCrAlY BC is to (1) increase the high-temperature oxidation/corrosion resistance of the underlying superalloy by the slow growing of a thin and stable Al_2O_3 -based thermally grown oxide (TGO) layer ($\sim 1\text{-}10$ μm) when the TBC is exposed to high temperatures, (2) increase the YSZ top coat adhesion to the component and (3) reduce residual stress due to the mismatch of coefficient of thermal expansion (CTE) values between the ceramic top coat and metallic part (Ref 3, 4).

The main role of the YSZ top coat is to provide an insulation heat flux barrier to avoid having the metallic parts reach their softening or melting temperatures. This is achieved due to the high melting point of the YSZ ($\sim 2700^\circ\text{C}$) and its low thermal conductivity values (< 2 W/mK) (Ref 3, 4).

The use of TBCs with internal cooling of the turbine metallic component and air film cooling of the TBC surface can provide reductions in the surface temperature of the metallic parts from ~ 100 up to $\sim 300^\circ\text{C}$ (Ref 3). Therefore, they allow advanced turbine engines to operate at gas combustion temperatures higher than the melting or softening points of the metallic superalloys, which are typically below 1400°C . In fact, according to Snecma, the maximum combustion chamber outlet temperature ($T_{\text{comb-out}}$) (a.k.a., turbine inlet temperature) of the M88 engine of the Rafale fighter jet is 1577°C (Ref 5). As a curiosity, APS YSZ TBCs have been tested in high heat flux (H_2/O_2) rocket engines by the National Aeronautics and Space Administration (NASA). The maximum gas combustion temperature reached was at the $\sim 1500^\circ\text{C}$ level according to Nesbitt (Ref 6), i.e., similar to that reported for the M88 Snecma jet engine. The overall TBC schematics are found in Fig. 1.

TBCs have the potential to improve engine efficiency by allowing higher turbine operating temperatures. For example, according to Perepezko (Ref 7), the specific core power of turbine engines is almost linearly proportional to $T_{\text{comb-out}}$ levels, from ~ 800 to $\sim 2000^\circ\text{C}$. Consequently, the maximum

Rogério S. Lima and Basil R. Marple, National Research Council of Canada, 75 de Mortagne Blvd., Boucherville, QC J4B 6Y4, Canada. Contact e-mail: rogerio.lima@cnrc-nrc.gc.ca.

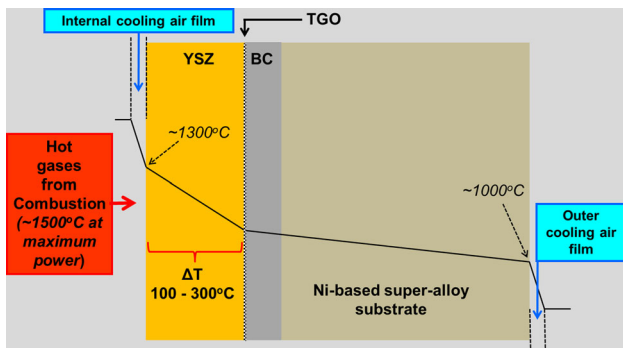


Fig. 1 Cross-sectional schematics of an air-cooled thermally sprayed TBC system on an engine component (e.g., combustion chamber)

$T_{\text{comb-out}}$ levels will be limited by material/metallurgical conditions, because the metallic superalloys typically employed in turbine engines will normally melt and/or soften below 1400 °C. Therefore, the development/availability of TBCs to allow higher $T_{\text{comb-out}}$ values is a must.

Nonetheless, although the performance of a turbine engine increases with temperature (Ref 7), environmental regulations will likely tend to curb further attempts to increase the combustion temperatures. This is related to keeping NO_x and CO levels within emission standards (Ref 8). The variations of CO and NO_x emission levels with combustion flame temperature were described by Lefebvre (Ref 9). At lower temperatures, the NO_x levels decrease substantially, but with a trade-off in the enhanced amount of CO emissions produced. On the contrary, at higher temperatures the CO emission levels are drastically reduced, but with a peak in NO_x emission levels. Therefore, there is a “sweet spot” of temperature levels when a compromise between NO_x and CO emissions is achieved, which is within the ~1400-1600 °C temperature range (Ref 9). Consequently, the next generation of turbine engines may need to work within this maximum temperature envelope.

This ~1400-1600 °C maximum temperature envelope is key regarding the durability of the TBC in service. The high-temperature (e.g., ~1400-1600 °C) stable phases of YSZ are the tetragonal (*t*) and cubic (*c*) phases. Upon cooling to room temperature (RT), the *c*-phase can keep its structure; however, the *t*-phase undergoes the known stress-induced martensitic transformation to the monoclinic (*m*) phase of YSZ. This martensitic transformation is accompanied by a volume expansion of 3-5%. Under controlled conditions, it leads to the so-called transformation toughening of the partially stabilized zirconia (PSZ), according to Stevens (Ref 10); however, on a large scale, it leads to material damage due to extensive micro-cracking (Ref 10). It needs to be highlighted that this phase transformation is reversible and cyclic, i.e., *t*-phase transforms into *m* upon cooling to RT and *m*-phase transforms into *t* upon heating from RT.

The current effective high-temperature capability limit of APS YSZ TBCs is mainly related to the phase transformations that occur with the tetragonal (*t'*) phase of the YSZ at high-temperature exposure. The so-called metastable or non-transformable *t'*-phase is formed during the rapid quenching (approximately 10⁶-10⁸ °C/s, as pointed out by Fauchais (Ref 11)) and solidification of the molten particles during thermal spraying (as-sprayed coating). It is important to highlight the fact that the *t'*-phase is a single phase throughout the YSZ coating; i.e., it is not a mixture of *t'* and other phases (unless

semi-molten particles are embedded in the coating microstructure). The formation of the *t'*-phase is inherent to the thermal spray process and any other technique that involves rapid YSZ solidification from the melt or vapor state.

It is important to point out that the *t'*-YSZ phase does not undergo the stress-induced martensitic transformation to the *m*-phase of YSZ when cooled from high temperature (e.g., 1500 °C) to RT. Therefore, the presence of the *t'*-phase in TBCs is highly desirable due to the lack of phase transformation, as pointed out by VanValzah and Eaton (Ref 12) and Brandon and Taylor (Ref 13). However, the *t'*-phase is in fact metastable, i.e., transforms slowly into the equilibrium tetragonal (*t*) and cubic (*c*) phases at temperatures $\geq \sim 1300$ °C (Ref 12, 13). Upon cooling from high temperature to RT, the *t*-phase transforms into *m*-phase, as well as, the *c*-phase. It needs to be stressed that the formation of the *m*-phase is detrimental to the mechanical integrity of the YSZ TBC, due to the volume changes (i.e., micro-cracking) that occur upon typical TBC thermal cycling, i.e., heating from RT to high temperature (*m* → *t*) and cooling from high temperature to RT (*t* → *m*) (Ref 12).

As the *t'*-phase begins its slow phase transformation to the *t*- and *c*-phases at ~1300 °C, this temperature is typically considered as the maximum temperature limit for YSZ regarding TBC operations. This is one of the main reasons why there is the need for air film cooling on the surface of TBCs in turbine parts (in addition to back cooling), to avoid the TBC reaching temperatures higher than ~1300 °C, as depicted in Fig. 1.

Although this paper is aiming at studying the maximum operation temperature limits of TBCs from the point of view of the YSZ top coat, the importance of the maximum operating temperature limits of the MCrAlY BC (~1150 °C) (Ref 14), which are fundamental for TBC performance, cannot be forgotten. Temperatures higher than ~1150 °C will lead to an unstable TGO formation, leading to a premature spallation of the YSZ top coat. Therefore, the need of obtaining a thermal gradient with a “steep slope,” to avoid exposing the BC to temperature levels similar to those of the YSZ top coat, is paramount for this type of study. This is necessary to minimize the BC contribution to the YSZ top coat failure.

The objective of this present work is to obtain preliminary data to check the validity of the current 1300 °C upper temperature limit of YSZ TBCs, specifically within the ~1400-1600 °C temperature range. To accomplish this objective, the thermal cycling performance of an “optimized” APS YSZ TBC (i.e., YSZ exhibiting low thermal conductivity levels at 1500 °C), operating at temperatures of ~1500 °C in a thermal gradient laser-rig, was evaluated. The 1500 °C temperature value for the YSZ was chosen based on the information available in the literature regarding the operating temperatures of TBC-protected engines (Ref 5, 6), as well as, for being midway within the “sweet spot” for lower emissions of NO_x and CO (Ref 9). In addition, the backside temperature levels of the substrate needed to stay at $\leq \sim 1000$ °C to minimize the MCrAlY BC contribution to the TBC failure, as previously stated.

2. Experimental Procedure

2.1 Thermal Spraying

The substrate material employed in this study was the single-crystal CMSX-4 metallic superalloy. The puck-shaped

substrates (2.5 cm (1") diameter and 3.2 mm (1/8") thick) were degreased and grit-blasted on both sides prior to thermal spraying. The NiCoCrAlY + HfSi BC (Amdry 386-4, Oerlikon Metco, Westbury, NY, USA) and the YSZ top coat (Metco 204B-NS, Oerlikon Metco, Westbury, NY, USA) feedstock powders employed in this study were sprayed using an APS torch (Metco 3 MB, Oerlikon Metco, Westbury, NY, USA).

The engineering of TBCs with lower thermal conductivity values (at high temperatures) than those currently employed will be paramount to either (1) increase the turbine power by increasing $T_{\text{comb-out}}$ or (2) reduce the amounts of NO_x and CO emissions by redirecting extra air (from cooling) to the combustion chamber. The YSZ TBC of this study was optimized to yield low thermal conductivity values at high temperatures. The complete set of spray parameters and the optimization process are considered as intellectual property (IP) of the National Research Council of Canada (NRC) and cannot be disclosed. The BC and YSZ top coat thicknesses were ~175 and ~425 μm, respectively.

2.2 Microstructural Characterization

In order to better preserve the microstructure, the as-sprayed TBC sample was vacuum impregnated in epoxy resin prior to cutting with a diamond saw. The mounted sample was then cut to produce a cross section, which was remounted in epoxy and polished according to standard metallographic procedures for TBCs. The cross-sectional microstructure was analyzed by scanning electron microscopy (SEM). The SEM pictures were taken in backscattered (BSE) mode. X-ray diffraction (XRD), using CuK α radiation in Bragg-Brentano configuration, was employed to evaluate the phase compositions of the YSZ powder and the as-sprayed and thermally cycled TBCs. The XRD 2 θ values ranged from 20° to 80° (scanning step size of 0.05° and step time of 2.5 s). The porosity of the TBC was measured on the cross section via optical microscopy (Eclipse ME600, Nikon, Tokyo, Japan) and image analysis (IA) software (Clemex Vision PE, Clemex Technologies Inc., Longueuil, QC, Canada) at a magnification of 200 \times ($n = 3$).

2.3 Thermal Diffusivity and Conductivity

The thermal conductivity values of as-sprayed and annealed YSZ TBCs were calculated using the traditional thermal conductivity (TC) equation: K (W/mK) = α (m²/s) \times C_p (kJ/kgK) \times d (kg/m³); where K is TC, α is thermal diffusivity (TD), C_p is the specific heat of the YSZ and d is the coating density.

The samples for TC measurements were free-standing YSZ coatings obtained by spraying the YSZ onto low carbon steel substrates. The as-sprayed coatings were detached from the substrates via acid dissolution and, subsequently, dried in a furnace at 150 °C for 12 h. The free-standing coatings were then annealed in air at 1300 °C (3 coatings) and 1500 °C (3 coatings) for 10 h in a box furnace (heating rate 300 °C/h and natural cooling to RT inside the furnace). The annealing was employed to guarantee that the microstructures would remain nearly stable prior to TD measurements at the same temperature levels (i.e., 1300 and 1500 °C).

The laser-flash technique (FlashLine 5000, Anter Corp., Pittsburgh, PA, USA) was employed to measure the TD values of the free-standing as-sprayed and annealed YSZ samples. For TD measurements, a ~1-2-μm-thick graphite layer (Graphite Spray Paint CX-01, TA Instruments, New Castle, DE, USA) was sprayed on the YSZ samples to increase the absorption of

the yttrium aluminum garnet (YAG) laser ($\lambda = 1.1 \mu\text{m}$) radiation energy and maximize the accuracy of the measurement of the infrared sensor. The TD measurements were taken at 1 atm (1 bar) with constant Ar gas flow of ~0.25 lpm. The TD values were measured at RT only for the as-sprayed coating and at different temperature intervals, from RT to 1300 °C and from RT to 1500 °C for the annealed ones. A total of three samples per YSZ coating were used for TD measurements.

The d values of the as-sprayed and annealed YSZ samples were measured via the Archimedes technique: d (kg/m³) = $(m_{\text{dry}}/(m_{\text{wet}} - m_{\text{immersed}})) \times 1000$; where m is mass in grams. A total of three samples per coating were used to generate the density values. It has to be highlighted that the d values of the as-sprayed and annealed coatings were measured at RT and used to calculate the RT and high-temperature TC values reported in this work.

The RT and annealed C_p values of the YSZ samples (at RT and high temperatures) were estimated based on the equation from the APS YSZ TBC database of Wang et al. (Ref 15):

$$C_p \text{ (kJ/kgK)} = (m_1 + m_2T + m_3T^{-0.5} + m_4T^{-2} + m_5T^{-3}) \times 1000;$$

where $m_1 = 0.600045$, $m_2 = 4.296 \times 10^{-5}$, $m_3 = 0.22845$, $m_4 = -24201$, $m_5 = 2.3668 \times 10^{-6}$ and T is the temperature in Kelvin.

2.4 Thermal Gradient Cyclic Testing Rig (a.k.a., Laser Rig)

The NRC thermal gradient laser rig is based on a 3-kW CO₂ laser, which produces a constant laser beam (10.6 μm wavelength) over the YSZ TBC top coat. The rig is set to create a laser spot size of about 2.5 cm (1") in diameter, in order to fit the dimensions of the substrate. A compressed air jet cools the backside of the substrate in order to generate the thermal gradient along the TBC/substrate profile. The rig is closed-loop computer-controlled; therefore, the temperature of the YSZ top coat (T_{front}) and the temperature of the un-coated backside of the substrate (T_{back}) are continuously recorded during the tests. This type of laser rig system has been previously developed at NASA by Zhu et al. (Ref 16) to test TBCs in gradient configuration. The overall schematic image of the rig is found in Fig. 2.

The temperature of the YSZ top coat was monitored using a one-color 7.9-μm wavelength pyrometer with a spot size of ~7 mm at the center of the sample. The temperature of the un-coated substrate backside was measured using a one-color 5.1-μm wavelength pyrometer with a spot size of ~4 mm at the center of the sample. An infrared (IR) camera (7.5-14 μm spectral range) coupled with a CO₂ notch filter at 8 μm was also employed to measure the overall distribution of temperature on the surface of the YSZ top coat. The IR camera is used to guarantee a uniform laser beam and temperature over the surface of the TBC. The emissivity value for the YSZ was measured and set as 0.96. It is important to highlight that this is the average value reported in the literature for an APS YSZ coating, at the 8-12 μm wavelength range (Ref 17).

A CMSX-4 substrate was grit-blasted to remove surface contaminants and subsequently oxidized in air for 1 h at ~1000 °C. After oxidation, a high heat enamel black spray paint (Tremclad, Rust-Oleum, Concord, ON, Canada) of known emissivity (0.96) was sprayed on half side (one half of one side was spray-painted, whereas the other half was left as is) of the 2.5 cm (1") diameter substrate. The laser rig was used to heat the sample, and the backside pyrometer emissivity was set to 0.96 to measure the temperature of the half-coated side. The

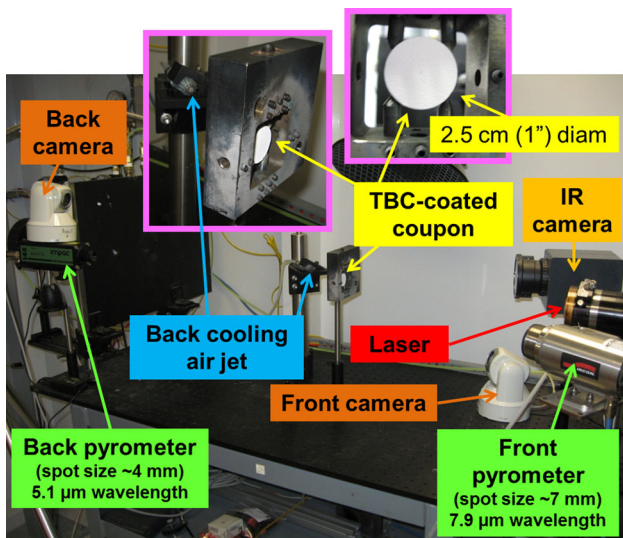


Fig. 2 Image of the thermal gradient laser-rig system of the NRC

laser-rig power was slowly increased until the backside of the substrate reached a temperature of ~ 600 °C, which is near the maximum operational temperature of the paint (650 °C). The pyrometer measurement zone was then switched to the half un-coated side, and the same laser power was applied on the sample. Then, the emissivity of the pyrometer was manually changed until the half un-coated backside exhibited a temperature of ~ 600 °C. The emissivity value found was 0.8, which has also been reported in the literature for an oxidized CMSX-4, from 650 to 1000 °C (Ref 18).

2.5 Thermal Gradient Cyclic Testing Modes

Two types of thermal gradient cycles were performed, short duration (5-min hot and 2-min cool—Fig. 3) and long duration (1-h hot and 2-min cool—Fig. 4). The substrate back-cooling air jet was set and fixed at a certain flow value (in liters per minute) nonstop during the entire testing. The laser power (in W) was initially increased manually until the YSZ TBC reached a surface temperature of ~ 1500 °C. After this temperature value was achieved, the laser power was set constant in cycles (5 min or 1 h). The “right” combination of laser power over the YSZ and air cooling on the substrate backside was “manually” chosen because it generated the desired T_{front} (YSZ) and T_{back} (CMSX-4 substrate) values of ~ 1500 °C (Ref 5, 6, 9) and ~ 1000 °C, respectively.

3. Results and Discussion

3.1 TBC Microstructure

A micrograph showing the overall as-sprayed TBC microstructure deposited on the CMSX-4 substrate is found in Fig. 5. No major cracking, debonding or delamination was observed. The YSZ top coat exhibited a lamellar micro-cracked morphology (intra-lamellar vertical cracks), with inter-splat and globular pores, which are desired for TBC applications. The BC exhibits a combination of splats, semi-molten particles and some oxides (dark grayish phases—atoms of lower atomic numbers appear darker in backscattered images).

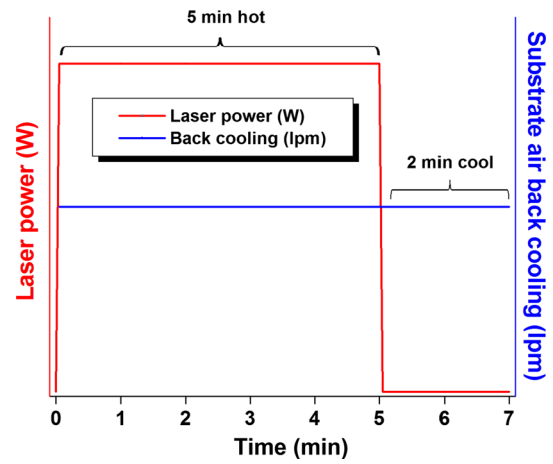


Fig. 3 Schematics of the short-cycle duration test

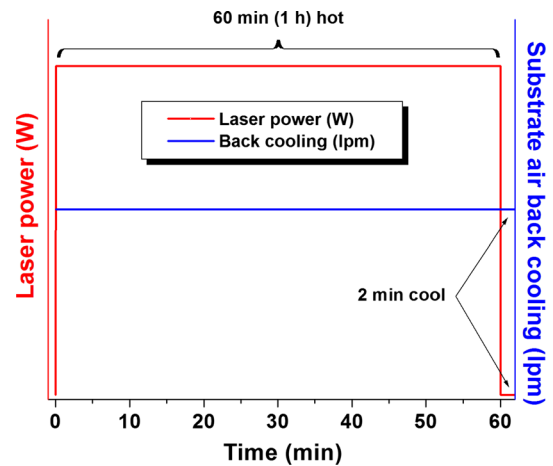


Fig. 4 Schematics of the long-cycle duration test

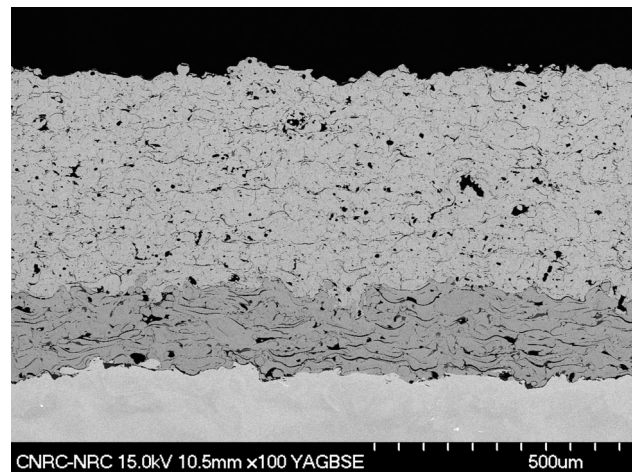


Fig. 5 Overall as-sprayed TBC microstructure on CMSX-4 substrate

The density values (measured via Archimedes method) of free-standing YSZ TBCs were ~ 5.2 g/cm³ (as-sprayed), ~ 5.3 g/cm³ (1300 °C-10 h) and ~ 5.4 g/cm³ (1500 °C-10 h). The fully dense YSZ value reported by Ingel and Lewis III is

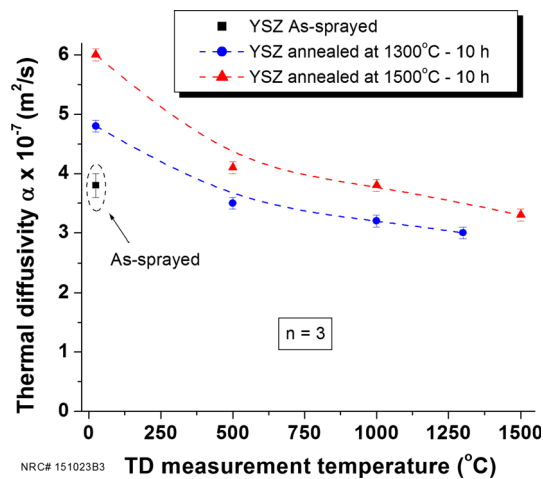


Fig. 6 Thermal diffusivity values of as-sprayed and annealed YSZ TBCs

6.03 g/cm³ (Ref 19). Using this value as reference, the porosity of the YSZ TBCs could be estimated to be ~14% (as-sprayed), ~12% (1300 °C-10 h) and ~10% (1500 °C-10 h). The porosity values measured via IA software (optical microscopy at 200X) of the BC (threshold manually set at 100) and YSZ (threshold manually set at 60) top coat were 13 ± 1% and 12 ± 1%, respectively.

3.2 Thermal Diffusivity and Conductivity Values

TD can be described as a measure of “how fast” heat propagates through the thickness of a material, whereas TC can be described as a measure of “how much” heat propagates through the thickness of the same material. Both quantities are proportional to each other, i.e., the higher the TD, the higher the TC at the same temperature (and vice versa).

The TD and TC values for the as-sprayed and annealed YSZ TBCs are found in Fig. 6 and 7, respectively. It is possible to observe that the TD values at RT of the annealed YSZ TBCs are higher than those of the as-sprayed one (~26% at 1300 °C-10 h and ~58% at 1500 °C-10 h) (Fig. 6). Regarding TC values at RT, they are ~0.7 W/mK for the as-sprayed YSZ, whereas they are ~0.9 and ~1.2 W/mK for the coatings annealed at 1300 °C-10 h and 1500 °C-10 h (Fig. 7). Therefore, the annealed YSZ TBCs exhibited an increase in TC values from the as-sprayed sample of ~30% (1300 °C-10 h) and ~70% (1500 °C-10 h) when measured at RT. As a curiosity, it has been reported by Schlichting et al. (Ref 20) that the average TC value for a fully dense bulk YSZ is ~2.0 W/mK from RT to 1000 °C.

This is the effect of sintering of the samples that occurred during the annealing process. As highlighted by McPherson (Ref 21), the true area of contact between two (as-sprayed) adjacent splats is about 20%, whereas the rest of the overall contact area is characterized by planar gaps of about 100 nm in thickness. This is the reason why as-sprayed thermal spray coatings exhibit lower TC values than those of bulk materials, even when both exhibit similar levels of coarse porosity (~1-20 μm of pore size, i.e., porosity that can be observed by optical microscopy or low magnification SEM ≤ 500X). Upon exposure to high temperatures, these nano-gaps sinter and heal, increasing the true contact area between two adjacent splats. As a consequence, the TD and TC values of thermal spray coatings

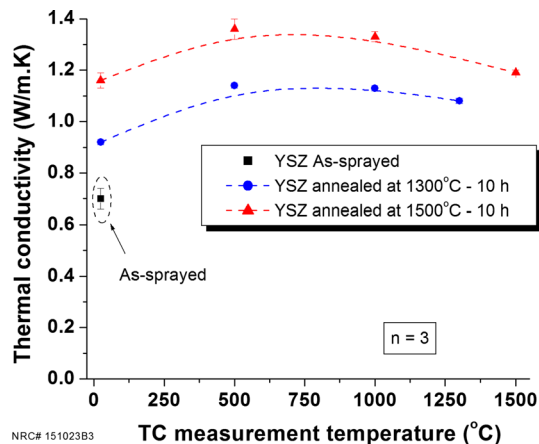


Fig. 7 Thermal conductivity values of as-sprayed and annealed YSZ TBCs

can increase substantially, even without necessarily showing a major effect on increasing coating density or reducing coarse porosity levels.

According to Carter and Norton (Ref 22), for a solid-state sintering (relative density >95%) to occur in a single-phase ceramic material (e.g., Al₂O₃) at 1 atm of pressure, the sintering temperature shall be at least ~80% of that of the melting point of the material. Following the ZrO₂-Y₂O₃ phase diagram, the melting point of the ZrO₂-8 wt.%Y₂O₃ (YSZ) is ~2700 °C (Ref 12, 13). Therefore, even at 1500 °C, the annealing temperature is ~55% that of the melting point of the YSZ, i.e., “too low” to produce a significant solid-state sintering effect. Consequently, the 70% increase in TC value at 1500 °C is likely related to the healing of these inter-splats nano-gaps, and not to a major densification. In fact as previously reported, the density values (Archimedes method) of the as-sprayed, 1300 °C-10 h and 1500 °C-10 h YSZ TBCs were approximately 5.2, 5.3 5.4 g/cm³, respectively.

Figure 6 shows that it is possible to notice that the TD values of the annealed YSZ TBCs maintained a steady decrease from RT up to 1300-1500 °C levels. It is also possible to observe that there are two slopes in the graph, (1) from RT to ~500 °C (higher slope) and (2) from ~500 °C to 1300-1500 °C (lower slope). This change of slope at ~500 °C for APS YSZ TBCs, which has been observed by Wang et al. (Ref 15), is likely related to the different contributions of heat transfer mechanisms to the overall heat transfer.

Heat transfer occurs through convection, conduction and radiation. In convection, heat is transferred by the motion of a gas or a fluid. Ratzer-Scheibe and Schulz (Ref 23) reported a ~10% increase in TC values for APS YSZ TBCs in Ar atmosphere when compared to vacuum (within the temperature range of RT-1200 °C), i.e., the presence of a gas inside the pores of the YSZ increases the TC of the TBC. Therefore, the convection effect is minimum for TBCs, but it cannot be neglected. Nonetheless, it cannot explain the lowering of TD values and/or the change of slope observed in Fig. 8.

In conduction, heat is transferred by means of collisions between rapidly moving free electrons (in metals), vibration of the chain molecules (in polymers) or the vibration of an array of atoms (i.e., lattice wave or phonon in ceramics). As YSZ is a ceramic material (i.e., low availability of free electrons), the heat conduction occurs by phonon transport, as highlighted by

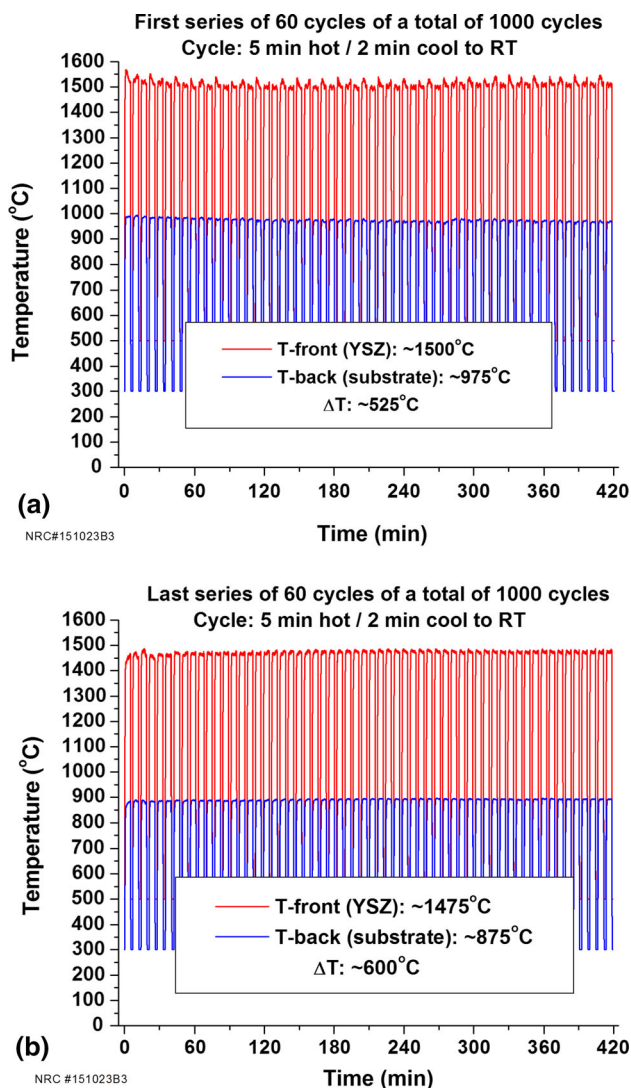


Fig. 8 (a) Short-duration cycles—first series of 60 cycles of a total of 1000 cycles. (b) Short-duration cycles—last series of 60 cycles of a total of 1000 cycles

Tan et al. (Ref 24) and Klemens and Gell (Ref 25). The phonons can be thought as being like sound or elastic waves. However, as the temperature increases, the scattering and interference of the adjacent lattice waves (phonons) are so intense that they tend to cancel each other, thereby causing the TC values to decrease. This can explain the overall decrease in TD values with temperature observed in Fig. 8 for the annealed YSZ TBCs.

At still higher temperatures, the radiant heat transfer becomes more prominent. In radiation, the heat is transferred via electromagnetic (radiation) waves. Infrared radiation (~1-1000 μm wavelength) heat may be transported through a transparent ceramic (for this wavelength range); and the heat transfer efficiency increases with temperature.

Therefore, the reduction (i.e., change) in TD slope observed for temperatures higher than 500 $^{\circ}\text{C}$ (Fig. 8) may be related to the contribution of radiation to increase the heat transfer capacity of the annealed YSZ TBCs, as hypothesized by Tan et al. (Ref 24).

Figure 7 shows that for the YSZ TBCs annealed at 1300 $^{\circ}\text{C}$ -10 h and 1500 $^{\circ}\text{C}$ -10 h, the TC values measured were ~1.1 W/mK (at 1300 $^{\circ}\text{C}$) and ~1.2 W/mK (at 1500 $^{\circ}\text{C}$), respectively. In order to make a fair comparison between these TC values and others reported in the literature, it is necessary to find APS YSZ TBCs for which the TC values were measured under similar conditions to those employed in this work. Tan et al. (Ref 24), using the same type of TC measuring procedure employed in this work (i.e., laser-flash method), reported APS YSZ TC values of ~1.3 W/mK measured at 1200 $^{\circ}\text{C}$ for a coating annealed at 1200 $^{\circ}\text{C}$ -10 h. Although this is not a large database, the TC values of the APS YSZ TBC developed for this study are lower than those reported in the literature, for similar TC measuring conditions. These low TC values also probably contributed to the “good performance” of these TBCs in thermal cycling, as shown in the next section. The low TC (in addition to a high YSZ thickness: ~425 μm) likely protected the BC, avoiding an unstable TGO growth, which leads to TBC premature failure.

Figure 7 shows that it is observed that for the annealed YSZ TBCs, the TC values were relatively stable at ~1.1 W/mK (1300 $^{\circ}\text{C}$ -10 h) and ~1.2 W/mK (1500 $^{\circ}\text{C}$ -10 h) from RT up to 1300 $^{\circ}\text{C}$ and 1500 $^{\circ}\text{C}$. Although the TD values tend to decrease with temperature, the APS YSZ C_p values (i.e., material’s ability to absorb heat from the environment) increase with temperature, as shown by Wang et al. (Ref 15). Therefore, they tend to balance each other (in the TC equation), thereby resulting in relatively stable TC values from RT to high temperatures.

It is important to point out that the main objective of this work was to observe the behavior of an APS YSZ TBC at high temperatures, including measuring the TD (and TC) values of an APS YSZ TBC at 1300 $^{\circ}\text{C}$ (current “standard” high-temperature limit for YSZ TBC operation) and at 1500 $^{\circ}\text{C}$ (potential higher-temperature limit based on Ref 5 and 7). Therefore, although Fig. 6 and 7 show the TD and TC values from RT to 1300-1500 $^{\circ}\text{C}$ in intervals of 500 $^{\circ}\text{C}$ for temperatures lower than 1000 $^{\circ}\text{C}$, these lower TD and TC temperature values (i.e., ≤ 1000 $^{\circ}\text{C}$) were measured not as a major objective, but rather as a quality control or “double-check.” Wang et al. (Ref 15) measured the TD and TC values of over 100 APS YSZ TBCs, from RT to 1400 $^{\circ}\text{C}$ in 100 $^{\circ}\text{C}$ intervals for scientific accuracy and precision. The TD and TC values reported in this work show similar behavior within the same temperature measurement range, which confirms that the APS YSZ TBC manufactured and tested in this study falls within the envelope of known behavior regarding thermal transfer properties.

3.3 Thermal Cycling

Regarding the short-duration cycles (5-min hot and 2-min cool), for the first 60 cycles of 1000 cycles, the *T-front* (YSZ) and *T-back* (substrate backside) values were ~1500 and ~975 $^{\circ}\text{C}$, respectively (Fig. 8a). For the last 60 cycles of 1000 cycles, the values were ~1475 and ~875 $^{\circ}\text{C}$ (Fig. 8b).

After 1000 cycles, the TBC was intact, as observed by the images of the as-sprayed and 1000X-cycled TBCs, as well as the YSZ IR camera image at the 1000th cycle (Fig. 9). If the TBC is spalling or about to spall, hot spots would appear in the IR camera picture. However, a well-distributed temperature is seen over the YSZ surface. It needs to be pointed out that for

this TBC the total time of high-temperature exposure at $\sim 1500\text{ }^{\circ}\text{C}$ was around 80 h (1000 hot cycles—5 min).

Throughout the 1000 cycles, the *T-front* temperatures remained almost unchanged at $\sim 1500\text{ }^{\circ}\text{C}$, whereas the *T-back* temperatures dropped from $\sim 975\text{ }^{\circ}\text{C}$ (Fig. 8a) to $\sim 875\text{ }^{\circ}\text{C}$ after 1000 cycles (Fig. 8b). This “counterintuitive” event has been reported for laser-rig testing of TBCs by Zhu et al. (Ref 16). Initially, the *T-front* levels tend to drop due to YSZ sintering effects, i.e., an increase in TC values leading to an improved heat transfer to the substrate. However, after a continuous high-temperature cycling, horizontal micro-cracks begin to propagate along the YSZ/BC interface due to TGO growth. These horizontal micro-gaps (1) reduce the heat propagation from the YSZ/BC interface to the metal substrate, (2) thereby counteracting the YSZ sintering effect (heat transfer to the substrate is now reduced and “bounces back” to the YSZ, i.e., resulting in no major changes at T-front overall) but (3) lowering the temperature of the backside of the substrate (as shown in Fig. 8b) (Ref 16).

Regarding the long-duration cycles (1-h hot and 2-min cool), after 10 cycles, the T-front (YSZ) and T-back (substrate backside) values were ~ 1450 and $\sim 950\text{ }^{\circ}\text{C}$, respectively (Fig. 10). After 10 cycles, the TBC was intact, as observed by the images of the as-sprayed and 10X-cycled TBCs, as well as the YSZ IR camera image at the 10th cycle (Fig. 11). It needs to be pointed out that for this TBC the total time of high-temperature exposure at $\sim 1500\text{ }^{\circ}\text{C}$ was 10 h (1 h hot \times 10 cycles).

It is important to highlight that for both types of cycles (i.e., short and long), the YSZ TBC T-front reached $\sim 1500\text{ }^{\circ}\text{C}$ levels after approximately 30 s of heating, whereas it reached RT after $\sim 100\text{ s}$ of cooling (Fig. 8a, b and 10). Therefore, the heating and cooling rates for the YSZ TBCs were ~ 50 and $\sim 15\text{ }^{\circ}\text{C/s}$, respectively.

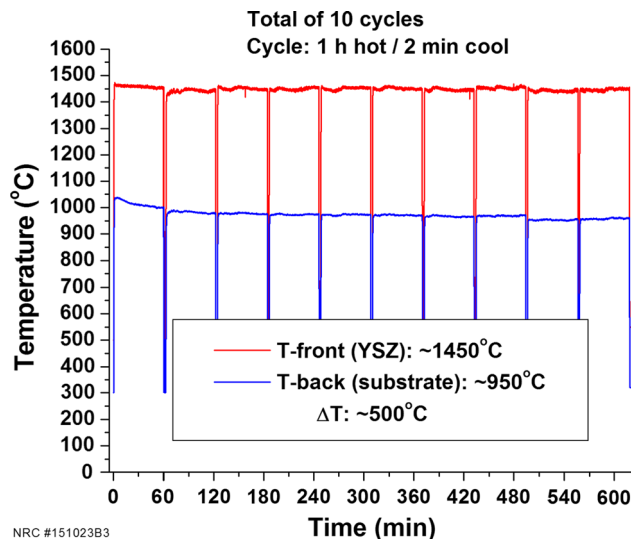


Fig. 10 Long-duration cycles—one series of a total of 10 cycles

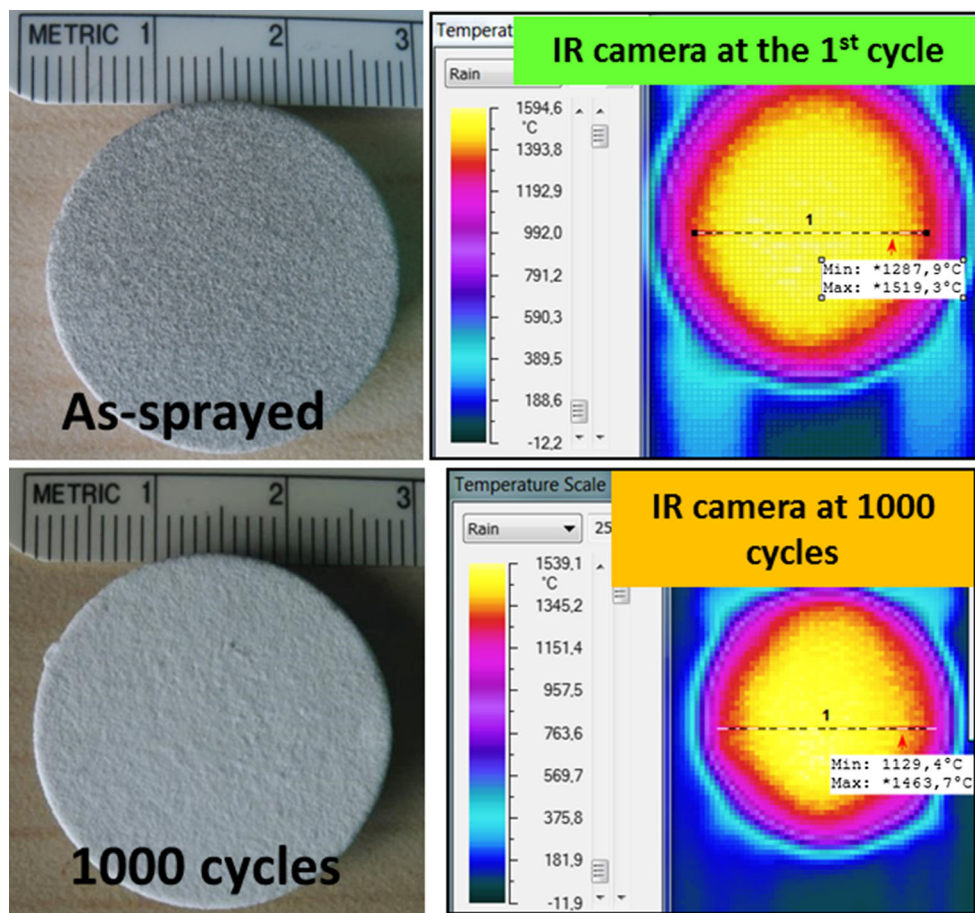


Fig. 9 Photograph images and infrared camera images of as-sprayed and thermally cycled ($\times 1000$) TBCs of Fig. 8

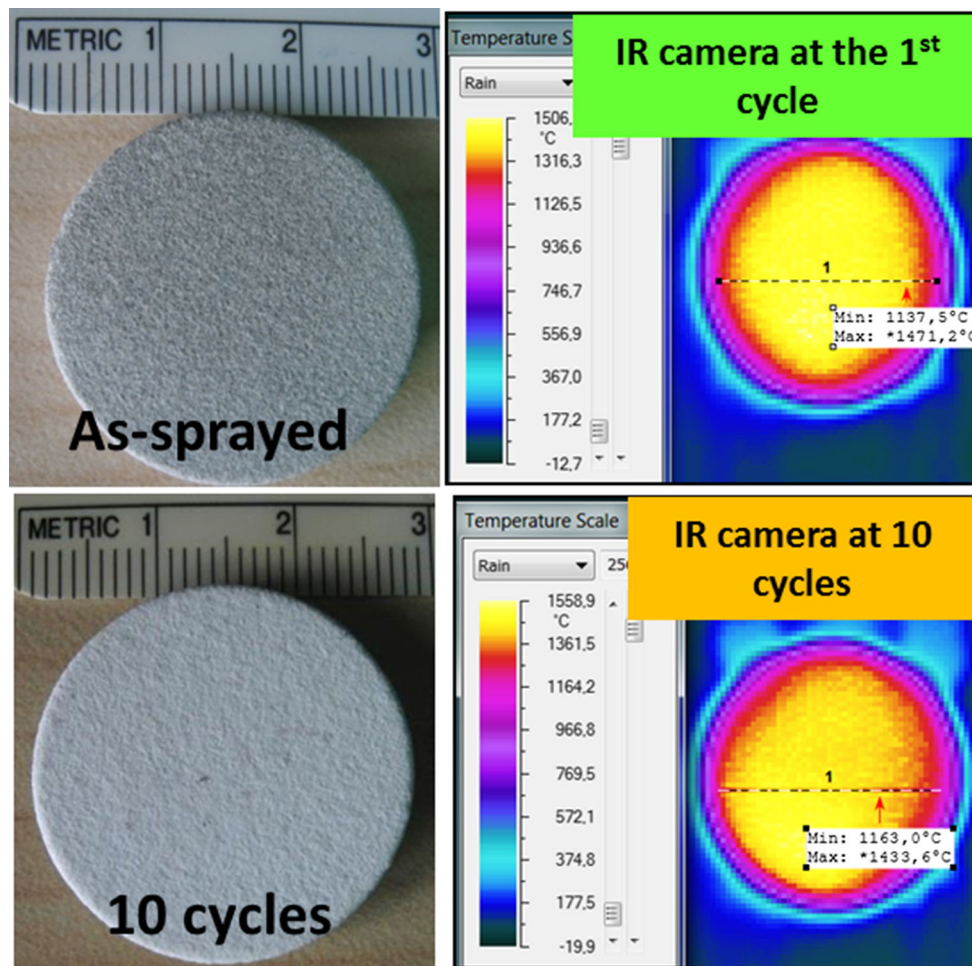


Fig. 11 Photograph images and infrared camera images of as-sprayed and thermally cycled ($\times 10$) TBCs of Fig. 10

The high thickness of the YSZ TBC ($\sim 425 \mu\text{m}$), in addition to the low YSZ TC value at 1500°C (Fig. 7), may have helped to avoid an unstable TGO formation. Therefore, TBC spallation and even early spallation signs were not observed (Fig. 9 and 11).

3.4 XRD Evaluation

The XRD peaks were identified based on the powder diffraction files (PDFs) provided by the International Centre for Diffraction Data (ICDD) (Newtown Square, PA, USA). The overall XRD patterns of the YSZ feedstock, as-sprayed and thermally cycled TBCs, are found in Fig. 12a. The presence of the t' -phase of YSZ is observed in the 2θ region from 72° to 76° of the XRD spectrum (Fig. 12b) (Ref 12). For the as-sprayed YSZ, it is possible to observe the two characteristic peaks of the t' -phase at $\sim 73.4^\circ$ (004) and $\sim 74.2^\circ$ (400) (PDF #17-0923), which is the desired phase for the YSZ for TBC applications, as previously reported (Ref 12, 13).

For the two cycled YSZ TBCs, it is possible to observe the slow phase transformation of the t' -phase into the t - and c -phases. This is observed by the decreasing or decay of intensity of the t' -phase peaks and the arising of the t -phase peaks at $\sim 73.1^\circ$ (004) and $\sim 74.4^\circ$ (220) (PDF #48-0224), as well as the c -phase at $\sim 73.5^\circ$ (400) (PDF #30-1468). It is important to point out that for both cycled coatings, the presence of the desired t' phase is still observed. The lack of spallation failure

of the cycled TBCs in this study is probably linked to the presence of that phase.

As previously stated, the formation of the m -phase is detrimental to TBC performance. The m -phase (PDF #37-1484), if present, is promptly observed in the 2θ region from 28° to 32° of the XRD spectrum (Ref 13). Surprisingly, the two highest intensity peaks (100% and 70%) of the m -phase at $\sim 28.2^\circ$ (-111) and $\sim 31.5^\circ$ (111) were not observed for the as-sprayed and cycled TBCs (Fig. 12c). The absence of the m -phase is probably another reason to explain the lack of spallation failure of the TBCs in this study. At $\sim 30.3^\circ$, the XRD peak can represent the c (111) (PDF #30-1468), t (101) (PDF #48-0224) or t' (111) (PDF #17-0923) phases.

The reason for the absence of the m -phase can be hypothesized based on the work of VanValzah and Eaton (Ref 12). APS YSZ TBCs were heat-treated in air in a furnace. The volume percentage of the m -phase in the as-sprayed coating was $\sim 4\%$. After an isothermal exposure at $\sim 1500^\circ\text{C}$ for 100 h, one TBC was air-quenched to RT and another one was gently cooled inside the furnace down to RT. The m -phase volume percentages for the air-quenched and furnace-cooled TBCs were ~ 12 and $\sim 48\%$, respectively (Ref 12). It was hypothesized that the high cooling rates (air-quenched TBC) contracted the coating structure, suppressing the $t \rightarrow m$ transformation, i.e., suppressing the volume expansion associated with this transformation via compressive residual stress (Ref 13).

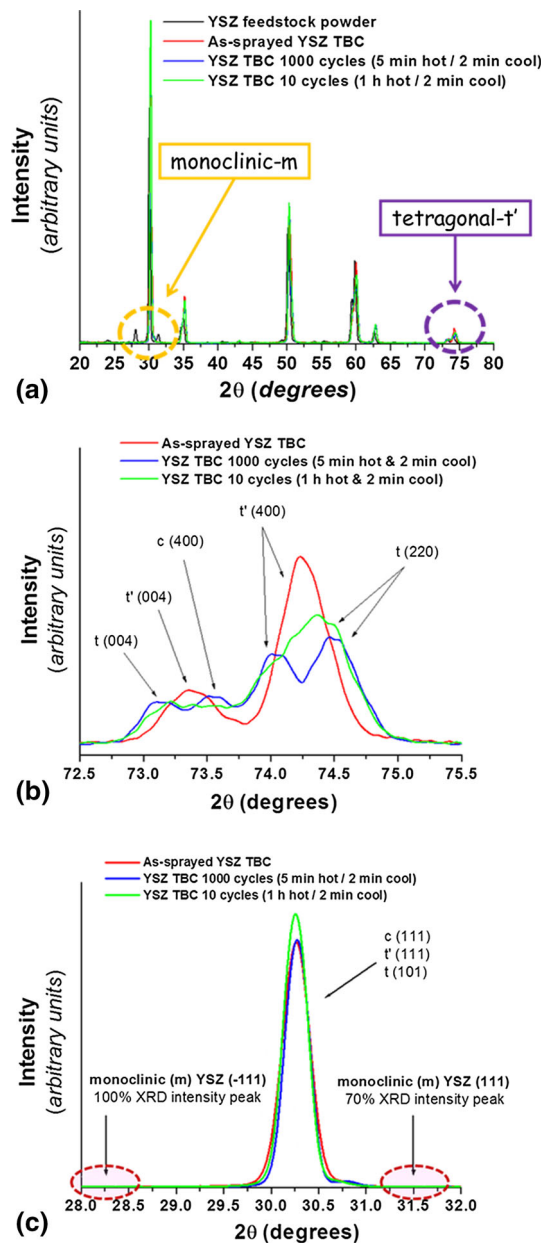


Fig. 12 (a) Overall XRD patterns of the YSZ feedstock powder, as-sprayed and thermally cycled TBCs. (b) Localized view of (a), highlighting the XRD region where the main t' -phase XRD peaks of YSZ appear. (c) Localized view of (a), highlighting the XRD region where the main m -phase XRD peaks of YSZ appear

Another hypothesis for the absence of the m -phase in the cycled coatings could be simply related to the lack of time (i.e., kinetics) for the t -phase to form the m -phase upon cooling to RT. As previously stated, during the laser-rig thermal cycling, the YSZ TBCs reached RT after 2 min of cooling (Fig. 8a, b and 10). This can be considered as a high cooling rate (when compared to furnace cooling), which may explain the absence of the m -phase for the cycled coatings.

3.5 Thermal Cycle Performance Comparison

As previously stated, the current high-temperature operational limit of YSZ APS TBCs is ~ 1300 °C, which is mainly associated with the phase transformations that occur at

temperatures higher than this level. These observations have been based on XRD studies for as-sprayed and heat-treated samples in furnaces (Ref 12, 13).

On a more practical level, in order to complement the furnace studies, it is interesting to observe the number of thermal cycles to failure of TBCs in thermal gradient cyclic rigs as a function of temperature (specifically T-front). These types of rigs, much more than furnaces, simulate the realistic operational environment of the hot zones of turbine engines (e.g., combustion chamber) in terms of temperature gradient, TBC structure and substrate material, as well as heating and cooling conditions (Ref 26). Therefore, this can be considered as a “relevant high-fidelity” test, which is paramount for achieving technology readiness level (TRL) of 5-6 (Ref 26, 27).

Table 1 shows the comparison of the number of thermal cycles to failure of TBCs in relation to the T-front values in thermal gradient cyclic rigs. The yellow row represents the results of the present work, whereas the green rows represent the results available in the literature (Ref 26, 28, 29). It is important to point out that in order to make a “fair comparison” all samples should exhibit: (1) same substrate shape (i.e., puck-shaped), (2) similar substrate dimensions (i.e., 25.4 diam \times 3.2 mm thick or 30 diam \times 3 mm thick), (3) similar BC thickness values (~ 150 -175 μ m), (4) similar top coat thickness values (~ 400 -500 μ m), (5) same top coat processing (i.e., APS), (6) same top coat composition (i.e., YSZ) and (7) same thermal cycle time (i.e., 5-min hot and 2-min cool).

The two red arrows in Table 1 (green rows) indicate that when T-front values increase from ~ 1240 to ~ 1450 °C, the number of cycles to TBC failure decreases from 4150 to 221, i.e., a reduction in approximately 95% in the number of cycles to spallation failure. It is important to notice that the T-back values in all cases are about 1000 °C.

It needs to be noted that the results of the current work are based on a thermal gradient created by a laser, whereas the results of the literature data of Table 1 are based on thermal gradients created by oxy-fuel flames, also known as burner rigs (Ref 26, 28, 29). When using a laser, the thermal energy is transferred to the TBC solely by radiation. In the case of an oxy-fuel flame, the thermal energy is mainly transferred via convection, although some radiation transfer is likely to occur. At this moment, it is too early to pinpoint how the results are affected, if they are affected, when using a laser or an oxy-fuel flame to generate the thermal gradient. Nonetheless, it is hypothesized that the kinetic energy of the burner-rig flame over the TBC surface may create an additional stress to the coating structure, thereby leading it to an early failure. In other words, the burner-rig testing probably more closely simulates the real environment of the turbine engine.

However, the cooling rate experienced by the laser-rig tested TBCs (T-front from high temperature to RT in 2 min) is at the same level as those experienced by the burner-rig tested TBCs listed in Table 1, and the spallation failure of TBCs typically occurs at the cooling stage (Ref 30).

Although there are still un-solved issues to be dealt with regarding the laser versus flame (i.e., burner rig) thermal gradient generation, Table 1 shows that an APS YSZ TBC has the potential to operate at T-front levels of ~ 1500 °C without exhibiting an early spallation failure.

3.6 Comment on BC Composition Effect

The BC material employed in this study (NiCoCrAlY + Hf + Si) may also have contributed to the “good

Table 1 Thermal gradient cycling test comparison—number of thermal cycles to failure of TBCs in relation to the T-front values in thermal gradient cyclic rigs

Puck-shaped substrate dimensions: diam x thick (mm)	Substrate material	BC (Processing) Thickness (μm)	Top coat (Processing) Thickness (μm)	Cycle time	T-front (°C)	T-back (°C)	Number of cycles	TBC failure (spallation)	Ref.
25.4 x 3.2	CMSX-4	NiCoCrAlY+HfSi (APS) ~175	YSZ (APS) ~425	5 min hot & 2 min cool	~1500	~1000	1000 (stopped)	No (0%)	Present work
30 x 3	Ni-based	CoNiCrAlY (not available) ~150	YSZ (APS) ~400	5 min hot & 2 min cool	~1450	~1050	221	Yes (20%)	27
30 x 3	Inconel 738	NiCoCrAlY (VPS) ~150	YSZ (APS) ~390	5 min hot & 2 min cool	~1350	~1010	1145	Yes (20%)	29
30 x 3	Inconel 738	NiCoCrAlY (VPS) ~150	YSZ (APS) ~420	5 min hot & 2 min cool	~1260	~1015	1200	Yes (20%)	29
30 x 3	Inconel 738	NiCoCrAlY (VPS) ~150	YSZ (APS) ~480	5 min hot & 2 min cool	~1350	~1020	1386	Yes (20%)	29
30 x 3	Inconel 738	NiCoCrAlY (VPS) ~150	YSZ (APS) ~500	5 min hot & 2 min cool	~1340	~1010	1692	Yes (20%)	29
30 x 3	Inconel 738	NiCoCrAlY (VPS) ~150	YSZ (APS) ~410	5 min hot & 2 min cool	~1260	~1015	1728	Yes (20%)	29
30 x 3	Inconel 738	NiCoCrAlY (VPS) ~150	YSZ (APS) ~450	5 min hot & 2 min cool	~1270	~1045	1733	Yes (20%)	29
30 x 3	Inconel 738	NiCoCrAlY (VPS) ~150	YSZ (APS) ~500	5 min hot & 2 min cool	~1240	~1000	3118	Yes (30%)	30
30 x 3	Inconel 738	NiCoCrAlY (VPS) ~150	YSZ (APS) ~410	5 min hot & 2 min cool	~1240	~1010	4150	Yes (30%)	30

performance” of the TBCs under laser cycle testing. According to the BC powder manufacturer (Amdry 386-4, Oerlikon Metco, Westbury, NY, USA), the powder composition is Ni (bal.wt.)/18-26 wt.%Co/13-21wt.% Cr/10-15wt.% Al/0.1-1wt.% Y/0.1-1wt.% Hf/0.1-0.7wt.% Si (Ref 31). Gupta and Duvall (Ref 32) compared the thermal cycle lives of electron beam—physical vapor deposition (EB-PVD) NiCoCrAlY versus LPPS NiCoCrAlY and LPPS NiCoCrAlY + HfSi BCs in burner rig testing (0.7 Mach gas velocity, 1-h cycle at 1150 °C). It was observed that all LPPS BCs exhibited improved cyclic oxidation life (from light oxide spall until substrate attack) when compared to the EB-PVD one. For the EB-PVD NiCoCrAlY BC, the substrate was attacked after 500 oxidation cycles, whereas for the best performing LPPS NiCoCrAlY + HfSi BC, the substrate was attacked only after 2000 cycles. The addition of silicon and hafnium in the MCrAlY LPPS BCs provided a synergistic improvement, leading to an enhanced oxide scale adherence (less oxide scale spallation) on the BC surface. The optimized LPPS BC composition exhibited the composition levels within those exhibited by the BC powder employed in this study. Therefore, the choice of the BC composition for this study may have contributed to the absence of TBC spalling during thermal cycle testing.

3.7 Thermal Gradient Cycle Performance of the TBC: Overall Hypothesis

Although there are still un-solved questions regarding the laser versus flame thermal gradient generation, Table 1 shows that an APS YSZ TBC has the potential to operate at T-front levels of ~1500 °C without exhibiting an early spallation failure. Based on the experimental results gathered in this paper, it is hypothesized that the (1) low thermal conductivity of the YSZ (~1.2 W/mK) at ~1500 °C and high YSZ thickness (400-500 μm range) (which may have avoided an unstable TGO formation on the BC), (2) the chemical composition of the BC (i.e., NiCoCrAlY + HfSi → enhanced adhesion of the TGO on the BC), (3) the presence of the *l'* phase in the cycled TBCs and (4) the rapid TBC cooling rates (T-front ~1500 °C to RT in 2 min), which led to (5) the absence of the monoclinic (*m*) phase in the cycled TBCs, probably contributed to this result.

4. Conclusions

The preliminary results of laser-rig thermal gradient testing have shown that a 400-500-μm-thick APS YSZ TBC, exhibit-

ing low thermal conductivity values at high temperatures (e.g., 1.2 W/mK at 1500 °C), may be able to operate above the 1300 °C temperature limit without an early catastrophic failure. APS YSZ TBC front temperature (*T-front*) and substrate backside (*T-back*) temperature levels of ~1500 °C and ~1000 °C, respectively, were achieved. No TBC spallation or even signs of spallation were observed after up to 1000 short cycles (5-min hot and 2-min cool) and 10 long cycles (1-h hot and 2-min cool). Further statistical evaluation (i.e., larger number of samples and longer testing time) is paramount to confirm these findings and gain more insight as to the implications of these results for industrial applications.

Although different ceramic TBC compositions are currently being studied by the thermal spray community, these preliminary results are promising regarding the potential to increase the effective high-temperature capability limits of APS YSZ TBCs. In other words, the state-of-the-art APS YSZ TBC may not have reached its full potential yet.

Acknowledgments

The authors would like to thank the immense help of the following Technical Officers of the NRC: Jean-Claude Tremblay for APS processing, David Delagrave for metallography prepping, Karine Théberge for SEM-XRD evaluation, Mario Lamontagne for thermal diffusivity measurements and Bernard Harvey/Mario Lamontagne for laser-rig engineering. Without you this work could not be accomplished. This R&D work was sponsored by the NRC (Factory of the Future Program) under the Surftec Thrust.

References

1. D.J. Wortman, B.A. Nagaraj, and E.C. Duderstadt, Thermal Barrier Coatings for Gas Turbine Use, *Mater. Sci. Eng. A*, 1989, **121**, p 433–440
2. X. Viot, A. Souchier, G. Dantu and F. Lassoudiere, High Thrust Engine Demonstrations (AIAA 2009-5132), in *45th AIAA/ASME/SAE/ASEE Joint Propulsion Conference & Exhibit*, Denver, Co, USA, 2009, p 1–8
3. N.P. Padture, M. Gell, and E.H. Jordan, Thermal Barrier Coatings for Gas-turbine Engine Applications, *Science*, 2002, **296**, p 280–284
4. A. Feuerstein, J. Knapp, T. Taylor, A. Ashary, A. Bolcavage, and N. Hitchman, Technical and Economical Aspects of Current Thermal Barrier Coating Systems for Gas Turbine Engines by Thermal Spray and EB-PVD: A Review, *J. Therm. Spray Technol.*, 2008, **17**(2), p 199–213
5. www.snecma.com/military-engines/training-and-combat-aircraft/m88. 12 January 2016
6. J.A. Nesbitt, Thermal Modeling of Various Thermal Barrier Coatings in a High Heat Flux Rocket Engine, *Surf. Coat. Technol.*, 2000, **130**, p 141–151
7. J.H. Perepezko, The Hotter the Engine the Better, *Science*, 2009, **326**, p 1068–1069
8. www.faa.gov/about/office_org/headquarters_offices/apl/research/aircraft_technology/clean/reports/media/TAPS_II_Public_Final_Report.pdf. 12 January 2016
9. A.H. Lefebvre, *Gas Turbine Combustion*, 2nd ed., Taylor & Francis, London, 1998
10. R. Stevens, Engineering Properties of Zirconia, *Engineered Materials Handbook—Vol 4: Ceramic and Glasses*, S.J. Schneider, Jr., Ed., ASM International, Materials Park, 1991, p 775–786
11. P. Fauchais, Understanding Plasma Spraying, *J. Phys. D Appl. Phys.*, 2004, **37**, p R86–108
12. J.R. VanValzah and H.E. Eaton, Cooling Rate Effects on the Tetragonal to Monoclinic Phase Transformation in Aged Plasma-sprayed Ytria Partially Stabilized Zirconia, *Surf. Coat. Technol.*, 1991, **46**, p 289–300
13. J.R. Brandon and R. Taylor, Phase Stability of Zirconia-based Thermal Barrier Coatings Part I: Zirconia-ytria Alloys, *Surf. Coat. Technol.*, 1991, **46**, p 75–90
14. J.A. Haynes, M.K. Ferber, and W.D. Porter, Thermal Cycling Behavior of Plasma-sprayed Thermal Barrier Coatings with Various MCrAlX Bond Coats, *J. Therm. Spray Technol.*, 2000, **9**(1), p 38–48
15. H. Wang, R.B. Dinwiddie, and W.D. Porter, Development of a Thermal Transport Database for Air Plasma Sprayed ZrO₂-Y₂O₃ Thermal Barrier Coatings, *J. Therm. Spray Technol.*, 2010, **19**(5), p 879–883
16. D. Zhu, S.R. Choi, and R.A. Miller, Development and Thermal Fatigue Testing of Ceramic Thermal Barrier Coatings, *Surf. Coat. Technol.*, 2004, **188–189**, p 146–152
17. L. Gonzalez-Fernandez, L. del Campo, R.B. Perez-Saez, and M.J. Tello, Normal Spectral Emittance of Inconel 718 Aeronautical Alloy Coated with Ytria Stabilized Zirconia Films, *J. Alloys Compd.*, 2012, **513**, p 101–106
18. S. Alaruri, L. Bianchini, and A. Brewinton, Effective Spectral Emissivity Measurements of Superalloys and YSZ Thermal Barrier Coating at High Temperatures using a 1.6 μm Single Wavelength Pyrometer, *Opt. Lasers Eng.*, 1998, **30**, p 77–91
19. R.P. Ingel and D. Lewis, III, Lattice Parameters and Density for Y₂O₃-stabilized ZrO₂, *J. Am. Ceram. Soc.*, 1986, **69**(4), p 325–332
20. K.W. Schlichting, N.P. Padture, and P.G. Klemens, Thermal Conductivity of Dense and Porous Ytria-stabilized Zirconia, *J. Mater. Sci.*, 2001, **36**, p 3003–3010
21. R. McPherson, A Review of Microstructure and Properties of Plasma Sprayed Ceramic Coatings, *Surf. Coat. Technol.*, 1989, **39**(40), p 173–181
22. C.B. Carter and M.G. Norton, *Ceramic Materials Science and Engineering*, Springer, New York, 2007
23. H.-J. Ratzer-Scheibe and U. Schulz, The Effects of Heat Treatment and Gas Atmosphere on the Thermal Conductivity of APS and EB-PVD PYSZ Thermal Barrier Coatings, *Surf. Coat. Technol.*, 2007, **201**, p 7880–7888
24. Y. Tan, J.P. Longtin, S. Sampath, and H. Wang, Effect of Starting Microstructure on the Thermal Properties of As-sprayed and Thermally Exposed Plasma-sprayed YSZ Coatings, *J. Am. Ceram. Soc.*, 2009, **92**(3), p 710–716
25. P.G. Klemens and M. Gell, Thermal Conductivity of Thermal Barrier Coatings, *Mater. Sci. Eng. A*, 1998, **245**, p 143–149
26. J. P. Feist, P. Y. Sollazzo, C. Pilgrim and J. R. Nicholls, Operation of a Burner Rig for Thermal Gradient Cycling of Thermal Barrier Coatings, in *Proceedings of the ASME Turbo Expo 2014, GT 2014*, June 16-20, Dusseldorf, Germany, GT2014-26325, pp. 1–10
27. http://www.nasa.gov/pdf/458490main_TRL_Definitions.pdf. 1 July 2016
28. M. Karger, R. Vassen, and D. Stover, Atmospheric Plasma Sprayed Thermal Barrier Coatings with High Segmentation Crack Densities: Spraying Process, Microstructure and Thermal Cyclic Behavior, *Surf. Coat. Technol.*, 2011, **206**, p 16–23
29. T. Steinke, D. Sebold, D.E. Mack, R. Vassen, and D. Stover, A Novel Approach for Plasma-Sprayed Coatings Tested Simultaneously Under CMAS and Thermal Gradient Conditions, *Surf. Coat. Technol.*, 2010, **205**, p 2287–2295
30. R.A. Miller and C.E. Lowell, Failure Mechanisms of Thermal Barrier Coatings Exposed to Elevated Temperatures, *Thin Solid Films*, 1982, **95**, p 265–273
31. http://www.oerlikon.com/ecomaXL/files/metco/oerlikon_DSMTS-009_3.4_NiCoCrAlY.pdf&download=1. 1 April 2016
32. D. K. Gupta and D. S. Duvall, A Silicon and Hafnium Modified Plasma Sprayed MCrAlY Coating for Single Crystal Superalloys, *Superalloys*, pp. 711–720 (1984). http://www.tms.org/Superalloys/10.7449/1984/Superalloys_1984_711_720.pdf. 1 April 2016